

# Influence of doping behavior of Al on nanostructure, morphology and optoelectronic properties of Al Doped ZnO thin film grown on FTO substrate

Marzieh Shirazi<sup>1</sup> · Reza Sabet Dariani<sup>2</sup> · Mohammad Reza Toroghinejad<sup>1</sup>

Received: 7 April 2016 / Accepted: 30 May 2016 / Published online: 13 June 2016  
© Springer Science+Business Media New York 2016

**Abstract** Al doped ZnO nanostructures deposited on FTO glass substrate by spray pyrolysis method with different Al doping levels (0–5 wt%). The structural, morphological, optical and electrical properties of fabricated samples were analyzed using X-ray diffraction (XRD), field emission scanning electron microscopy (FESEM), atomic force microscopy (AFM), photoluminescence (PL), four point probe, and UV–Vis spectroscopy. The results obtained from XRD analysis indicated that the growth preferred orientation of the ZnO thin films strongly depend on Al doping value. Also the crystalline plane distance and grain size decreased while free electron density and energy band gap enhanced as the Al doping value increased. PL analysis revealed the Near Band emission in PL spectra shifts to shorter wavelengths and Fermi surface shifts to conduction band with increasing the Al content. Electrical measurements illustrated that the resistivity reduces with doping Al into ZnO and reaches to minimum value for 3 % Al doped sample. Also the surface morphology and surface roughness of samples deposited by various Al doping values studied by FESEM and AFM analyzes.

## 1 Introduction

Zinc oxide (ZnO) is one of the technological semiconductor materials due to its interesting properties such as wide optical band gap (3.37 eV) at room temperature, high transparency, large exciton energy (60 meV), high chemical stability, and wide range of resistivity which can extend from  $10^{-4}$  to  $10^2 \Omega \text{ cm}$  [1–3]. ZnO-based structures have been applied in a variety of fields such as light emitting diodes, photo diodes [4], solar cells [5, 6], gas sensor [7], surface acoustic wave devices [8], field effect transistor [9] and piezoelectric devices [10].

ZnO has a wurtzite crystal structure and exhibits n-type conductivity which might be caused by intrinsic defects, oxygen vacancies and zinc interstitials. The conductivity of ZnO thin films can be enhanced by the substitution of Zn with various elements such as Al, Ga, In [11], Ta, Ni, Sn [12, 13] and Cu [14]. Al is preferable as a dopant source because ionic radius of  $\text{Al}^{3+}$  ion (0.54 Å) is much smaller compared to  $\text{Zn}^{2+}$  (0.74 Å) then it is more suitable to occupy the interstitial site [15]. Al doped ZnO thin films have low electrical resistivity and high transmittance in the visible region. The electrical conductivity and thermal stability of ZnO thin films can be improved by doping of Al. Also the optical band gap of ZnO can be controlled by Al doping amount [4]. Hence, it is important to investigate the influence of the dopants on the structural, optical, and electrical properties of ZnO nanostructure prior to employing these materials in practical applications [6, 7]. Some researchers are investigated the effect of Al doping value on different properties of ZnO nanostructure grown by different deposition techniques so far, including molecular beam epitaxy [4], hydrothermal method [11], chemical vapor deposition [16], pulsed laser deposition [17], sol–gel process [5], magnetron sputtering [18], electro

✉ Mohammad Reza Toroghinejad  
toroghi@cc.iut.ac.ir

Marzieh Shirazi  
marzieh.shirazi@ma.iut.ac.ir

Reza Sabet Dariani  
dariani@physics.queensu.ca

<sup>1</sup> Department of Materials Engineering, Isfahan University of Technology, Isfahan 84156-83111, Iran

<sup>2</sup> Department of Physics, Alzahra University, Tehran 1993893973, Iran

deposition [19], and spray pyrolysis [4, 20]. Among them, spray pyrolysis technique is considered as an inexpensive, reproducible and particularly useful method for the growth of nanostructures on large area substrates at low temperatures. Also control of dopant concentration in this method is simple with respect to other techniques [21, 22].

As it was previously mentioned, ZnO nanostructures can be used as a window layer, electrodes on hydrogenated amorphous silicon based solar cells and dye sensitized solar cells [23]. AZO nanostructures have appeared as an attractive option in the design of transparent electrodes in thin films solar cells due to the simultaneous occurrence of high transmittance in the visible region and low resistivity [5].

ZnO has the similar energy band structure and physical properties with  $\text{TiO}_2$  which frequently use as photo anode in dye sensitized solar cell. However ZnO electron mobility is higher than  $\text{TiO}_2$  which will help to improve the efficiency of photo generated electron transfer and decrease the electron recombination probability. As regards the electrical conductivity of AZO thin film is higher than ZnO film, it is expected to exhibit reduced recombination and the enhancement of photocurrent with faster electron transport in AZO nanostructures. As a result, the efficiency of dye sensitized solar cells improve using the Al doped ZnO as a photoanode [5, 6]. Consequently, study of optical and electrical properties variations of Al doped ZnO seems to be useful for improvement of photovoltaic properties in dye sensitized solar cells.

In the recent years, many researchers are investigated Al concentration effect on the optical and the electrical properties of AZO thin films. Gurbuz et al. [15, 24] investigated the effect of the annealing temperature and Al concentration on the optical and electrical properties of the ZnO and AZO thin films deposited on the  $\text{SiO}_2$  substrate. Park et al. [25] studied electronic structure of AZO thin film which was deposited by ALD method on  $\text{SiO}_2$  substrate as a function of Al concentration. Al-Ghamdi et al. [26] studied the optical and structural properties of AZO thin films which were deposited on glass substrate by spin coating method. Although the AZO thin films properties have been studied by many researchers, but there are few experiments which are investigated properties of AZO thin film deposited on FTO substrate. Thus a comprehensive study on Al concentration effect on the structural, optical and electrical properties of AZO thin films deposited on FTO substrate can receive much attention.

In the present work, AZO thin films are deposited on FTO substrate by spray pyrolysis method and their structural, optical and electrical properties are comprehensively investigated as a function of Al doping levels. Deposition of AZO thin films on FTO substrate using spray pyrolysis method as a cheap and easy technique could be used for

fabrication of solar cells in commercial scale in the next future. The main goal of the present research is the Al concentration effect on the structural, morphological, optical and electrical properties of AZO thin film deposited by spray pyrolysis method. Some important parameters of these deposited thin films such as optical transmittance, band gap, electrical resistance, charge carriers concentration, carrier mobility, grain size and surface roughness as a function of Al concentration are measured and compared with similar reported results.

## 2 Experimental details

Undoped and Al doped ZnO nanostructures were deposited by spray pyrolysis method. The used spraying set up was a homemade system that we were developed in our lab to perform a uniform spraying sample. The spray solution was prepared by dissolving zinc acetate (Merck) in a mixture of deionized water and methanol with the ratio of 1:3. A few drops of acid acetic were added to the solution in order to prevent the formation of zinc hydroxide. Aluminum chloride was used as the source of dopant. The dopant concentration (Al/Zn at.%) was varied from 0 to 5 at.% and the concentration of precursor solution was 0.2 M. Also compressed ambient air was used to atomize the solution and the flow rate was kept 3 ml/min during preparation of samples. The nozzle to substrate distance was maintained at 15 cm and the substrate temperature was  $450 \pm 5$  °C which controlled using an electronic temperature controller K-type thermocouple. The substrate was a FTO coating glass with resistivity of  $15 \Omega/\text{sq}$  and thickness of 200 nm, which was cut in the dimensions of  $10 \times 10 \times 2 \text{ mm}^3$ . Initially the substrates ultrasonically cleaned in acetone, ethanol, and distilled water respectively and then dried in air.

The crystalline structures of the films were determined using a Philips diffractometer (Xpert pw3373) with a step size of  $0.02^\circ$  and count time of 1.0 s per step. Morphological properties of deposited samples were investigated by field emission scanning electron microscope (FESEM, Hitachi S-4160) and atomic force microscopy (AFM, Auto Probe Pc; in contact mode, with low stress silicon nitride tip of less than 200 Å radius and tip opening of  $18^\circ$ ) analysis. Also the thickness of the films were measured by cross-sectional FESEM images and found to be 10 and 200 nm for AZO thin film and FTO substrate, respectively. The optical transmittance spectrum of the films was measured in the wavelength range of 300–1100 nm by a high resolution spectrophotometer (Camspec, Model M350). Also the photoluminescence (PL) spectra were measured using a Cary Eclipse (Model: Stellar Net EPP-200) spectroscopy at room temperature. In this analysis, the He-Cd

laser (325 nm) was used as the excitation source. The sheet resistance was measured with four point probe system (Yasaleh model FPP02). The carrier concentration and carrier mobility were determined in the Van der Pauw configuration, using a Hall effect measurement system.

### 3 Results and discussion

#### 3.1 Structural properties

The X-ray diffraction (XRD) pattern of AZO thin films deposited on FTO substrates with different Al doping values are shown in Fig. 1. The respective positions of ZnO diffraction peaks show that all the films are polycrystalline with ZnO hexagonal wurtzite structure. For all ZnO diffraction peaks, the respective positions of peaks are in suitable agreement with the Joint Committee for Powder Diffraction Standards (JCPDS) standard data for ZnO powder (See JCPDS Card no: 00-036-1451).

All the films have a polycrystalline structure as indicated by the emergence of the ZnO (100), ZnO (002), ZnO (101), ZnO (102) and ZnO (103) peaks (see Fig. 1). No peaks observed related to the other compounds such as  $\text{Al}_2\text{O}_3$  phase in the XRD patterns, which indicates that Al atoms substitute Zn in the ZnO lattice and Al ions may occupy the interstitial sites of ZnO or segregates to the non-crystalline region in grain boundaries and forms Al–O bond.

From Fig. 1 it is observable that the (002) diffraction peak of AZO thin films is shifted to larger angle as compared to undoped ZnO thin film. The displacement of (002)

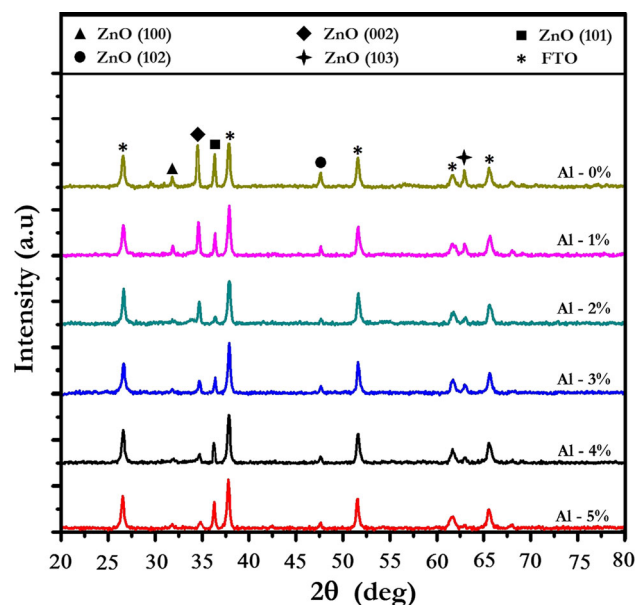


**Fig. 1** XRD patterns of the thin films deposited with different Al content

diffraction peak to larger angle may be attributed to substitution of  $\text{Zn}^{2+}$  ions by  $\text{Al}^{3+}$  ions at ZnO lattice sites [20, 27].

The inset in Fig. 2 shows the variations of diffraction angle and the crystalline plane distance ( $d$ ) value of the ZnO (002) diffraction peak as a function of Al doping content. As it is observable from Fig. 2, with enhancement of Al doping level the ZnO (002) peak position shifts to larger angle while the crystalline plane distance value decreases. Since  $\text{Al}^{3+}$  has a smaller ionic radius with respect to  $\text{Zn}^{2+}$ , the substitution of  $\text{Zn}^{2+}$  ions by  $\text{Al}^{3+}$  ions results in the decrease in the crystalline plane distance [16]. With substitution of a smaller ion instead of bigger one, lattice distance reduces and according to Bragg law  $2d \sin \theta = n\lambda$ , the diffraction angle increases. Therefore, the increasing of the diffraction angle corresponds to a reduction in the crystalline plane distance ( $d$ ).

The same results were reported by Park et al. [28] and Benzarouk et al. [29] for Al doped ZnO. Also, similar behavior is seen for ZnO doping with other elements such as Ta [12] and Ni [13].

The average crystallite size is estimated with the help of Scherrer's relation [30]:

$$D = k\lambda / \beta \cos \theta \quad (1)$$

where  $k$  is a constant,  $\lambda$  is the X-ray wavelength,  $\beta$  is the full width at the half maximum (FWHM) in radian of the peak and  $\theta$  is the Bragg diffraction angle. The average crystallite size of the AZO thin films with the variety of Al content from 0 to 5 % are shown in Fig. 2. From Fig. 2 it is observable that the average crystallite size decreases from 56.2 to 31.8 nm with increasing of Al doping level from 0 to 5 %. The reduction of crystallite size with increasing the

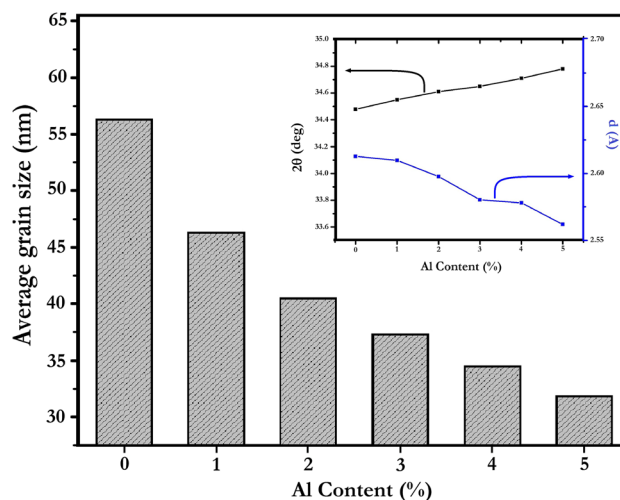


**Fig. 2** The variations of the average grain size, interplanar spacing ( $d$ ) and peak position of ZnO (002) versus Al content

Al doping value may be due to the substitution of Zn<sup>2+</sup> ions by Al<sup>3+</sup> ions in crystalline structure.

Figure 3 shows the intensities of ZnO (002) and ZnO (101) diffraction peaks as a function of Al doping levels. From Fig. 3 it is observable that the intensities of the all ZnO diffraction peaks are decreased when Al is doped in ZnO. However, when the Al doping level reaches to 3 %, the ZnO (101) peak intensity has an increase, indicating a change in the preferred crystalline orientation of the AZO thin films.

In order to investigation of the Al doping effect on the preferred orientation of the AZO thin films, the texture coefficient for the AZO thin films was calculated using relative texture coefficient via the following equation [30]:

$$TC(hkl) = \frac{I(hkl)/I_0(hkl)}{\frac{1}{N} \sum I(hkl)/I_0(hkl)} \quad (2)$$

where TC (hkl) is the relative texture coefficient of diffraction peaks, I (hkl) is the measured relative intensity of a plane (hkl), I<sub>0</sub> (hkl) is the standard intensity of plane (hkl) according to the JCPDS card 36-1451 and N is the reflection number of diffraction peaks. A sample with randomly oriented crystallite yields TC (hkl) = 1, while if TC (hkl) be more than one, it means that population of grains at (hkl) orientation is high, and for 0 < TC(hkl) < 1 values a few grains are grown at (hkl) orientation.

The calculated texture coefficients for ZnO (002) and ZnO (101) diffraction peaks are listed in Table 1. For undoped ZnO thin film, the values of the TC (002) and TC (101) were found to be 1.54 and 1.24, respectively. This result reveals that undoped ZnO thin film has a

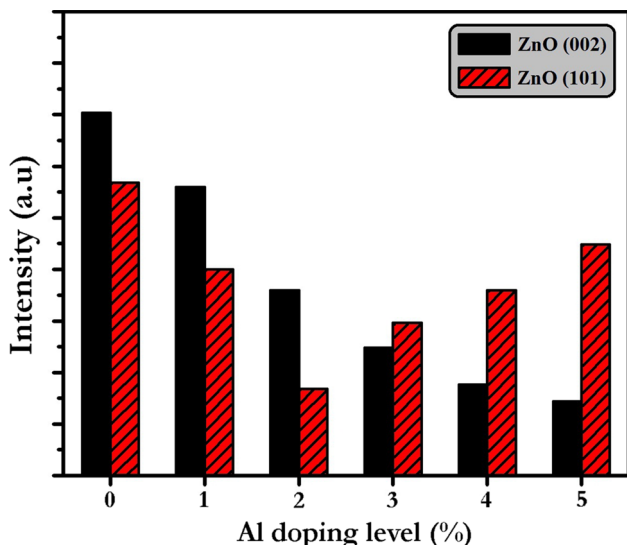


Fig. 3 The relative intensities of (002) and (101) ZnO diffraction peaks as a function of Al content

polycrystalline structure with (002) ZnO preferred orientation. The presented results in Table 1 indicate that with increasing of Al doping level from 0 to 5 %, the value of TC (002) decreases from 1.54 to 0.91. On the other hand, with the enhancement of Al doping level from 0 to 2 % the value of TC (101) reduces from 1.24 to 1.19 while it increases from 1.73 to 2.32 with further increasing of Al doping level from 3 to 5 %. These results are in reasonable agreement with variations of intensities of ZnO (002) and ZnO (101) diffraction peaks presented in Fig. 3. Also results presented in Table 1 reveal the replacement of preferential orientation from (002) to (101) ZnO plane, when the Al doping level reaches to 3 %.

These results are in perfect agreement with reported results by Castaneda et al. [31] which showed that at low Al doping samples, the doping have no effect on (002) growth orientation, while at high Al doping samples, growth preferred orientation is changed from (002) to (101).

It is clear that the Al doping value plays an important role in the crystallinity of the AZO thin films. The variation of growth orientation from (002) to (101) may have three reasons; firstly the enhancement of stacking defects and periodic loss in ZnO lattice, secondly segregation of Al around the grain boundaries [21, 22] and thirdly the change of intrinsic strain through doping [32, 33].

In the present study, the variation of intrinsic strain through doping leads to change of lattice constants, due to the smaller ionic radius of Al<sup>3+</sup> (53 pm) as compared to Zn<sup>2+</sup> (74 pm). It is important to analysis the strain, because it affect significantly the structural properties of AZO thin films. The mean strain for ZnO thin films with wurtzite structure can be obtained by the following formula [34]:

$$e_{zz} = (c - c_0)/c_0 \quad (3)$$

where e<sub>zz</sub> is the mean strain in ZnO thin films, c is the lattice constant of the ZnO thin films, and c<sub>0</sub> is the lattice constant of bulk (standard c<sub>0</sub> = 0.5206 nm). Also it is important to note that the lattice constant c of the (002) plane is calculated using the following equation [30]:

$$\frac{1}{d^2} = \frac{4}{3} \left( \frac{h^2 + hk + k^2}{a^2} \right) + \frac{l^2}{c^2} \quad (4)$$

where a and c are the lattice constants and d is the crystalline plane distance for indices (hkl) which is obtained from the XRD patterns.

The lattice mismatch in AZO crystalline structures can be related to degrees of stress during the deposition process of AZO thin films. For hexagonal crystals, the stress in the crystalline plane of the film (σ) can be calculated by the biaxial strain model [35]:

$$\sigma = (2c_{13} - (c_{11} + c_{12})(c_{33}/c_{13}))e_{zz} \quad (5)$$

**Table 1** Lattice parameter (a and c), texture coefficient for (002) and (101) planes, strain and stress for AZO thin films with different Al doping levels

| Al content (%) | lattice parameters (Å) |       | TC (002) | TC (101) | Strain (%) | Stress (GPa) |
|----------------|------------------------|-------|----------|----------|------------|--------------|
|                | a                      | c     |          |          |            |              |
| 0              | 3.247                  | 5.205 | 1.54     | 1.24     | −0.019     | −0.082       |
| 1              | 3.241                  | 2.203 | 1.29     | 1.15     | −0.057     | −0.247       |
| 2              | 3.237                  | 5.200 | 1.14     | 1.19     | −0.115     | −0.494       |
| 3              | 3.228                  | 5.198 | 1.03     | 1.73     | −0.153     | −0.659       |
| 4              | 3.226                  | 5.196 | 0.98     | 2.30     | −0.192     | −0.823       |
| 5              | 3.224                  | 5.195 | 0.91     | 2.32     | −0.211     | −0.906       |
| JPDS card      | 3.250                  | 5.206 |          |          |            |              |

where  $C_{ij}$  ( $i, j = 1, 2, 3$ ) are elastic stiffness constants. For ZnO thin films  $C_{13}$ ,  $C_{11}$ ,  $C_{12}$  and  $C_{33}$  are 106.1, 207.0, 117.7 and 209.5 GPa, respectively [35].

The strain and stress of AZO thin films calculated by Eqs. 3 and 5 are presented in Table 1. The negative sign for the calculated stress for all samples indicates that  $c < c_0$ , so the crystallites are in a state of compressive stress. Also, from Table 1 it is observable that the stress enhances as the Al concentration increases.

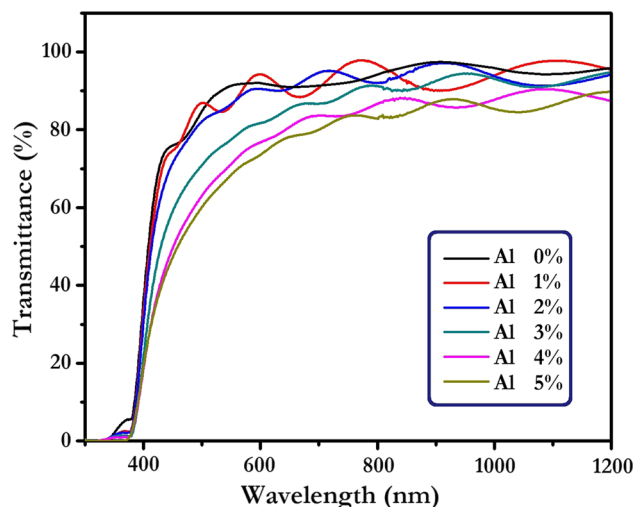
In brief, when  $Al^{3+}$  ion located in  $Zn^{2+}$  ion sites, because of smaller ionic radius of substitution element ( $Al^{3+}$  ion) with respect to host element ( $Zn^{2+}$  ion), the crystalline plane distance (d) reduced and according to Bragg formula, diffraction angle ( $\theta$ ) increased, thus (002) ZnO peak location shifted to higher angles. At low Al doping value,  $Al^{3+}$  ions could not seriously change the growth orientation in the lattice, but with the increasing of Al doping value, the substitution  $Al^{3+}$  ions in  $Zn^{2+}$  sites limited ZnO atoms growth at (002) orientation. Thus ZnO atoms grown at other crystal planes such as (101) orientation, as it is reported by other researchers [36, 37].

### 3.2 Optical properties

Figure 4 exhibits the optical transmittance of the AZO thin films deposited with various Al doping values from 0 to 5 %, in the range of UV–Vis wavelength (300–1200 nm). As can be seen from transmittance spectra, the average optical transmittance exceeds 85 % in the visible wavelength range.

From Fig. 4 it is observable that the transmittance of AZO thin films in the visible region decreases as the Al doping level increases. The reduction of the transmittance can be attributed to scattering from the grain boundary. Moreover, the crystal defects increase when  $Al^{3+}$  ions are introduced in ZnO lattice, resulting in the enhancement of photons scattering. Similar results are also reported by Prajapati et al. [37] and Dghoughi et al. [39].

In order to study the Al doping effect on the optical properties, the absorption edge of the AZO thin films is investigated. The absorption coefficient,  $\alpha(\lambda)$ , is defined as:

**Fig. 4** Optical transmittance spectra of samples deposited with different Al content

$$T = \exp[-\alpha(\lambda)t] \quad (6)$$

where T is the optical transmittance and t is the thickness of AZO film. The optical band gap is calculated by the following relationship [40],

$$\alpha hv = A(hv - E_g)^n \quad (7)$$

where  $hv$  is the photon energy,  $E_g$  is the optical band gap and A is a constant. Also the value of n depends on the probability of transition. It takes values as 1/2, 3/2, 2 and 3 for direct allowed, direct forbidden, indirect allowed and indirect forbidden transition, respectively. For direct band gap semiconductors like ZnO, the value of n is 1/2. The optical band gap obtain by plotting the  $(\alpha hv)^2$  versus  $(hv)$  which extrapolating the straight linear portion of this plot to the photon energy  $(hv)$  axis would give the optical band gap value.

Figure 5 shows the variation of  $(\alpha hv)^2$  versus  $(hv)$  used for calculating of the optical band gap. The optical band gaps determined from these curves are listed in Table 2. The optical band gap energy is found to be 3.14 eV for pure ZnO thin films. It can be seen that the optical



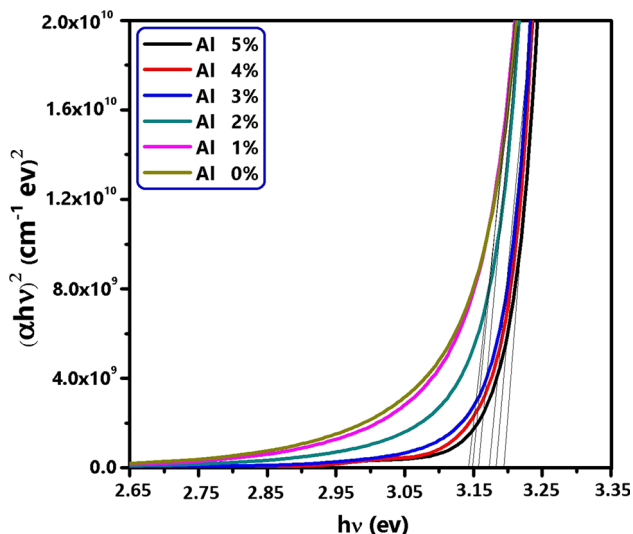


**Fig. 5** The plot of  $(\alpha hv)^2$  versus  $(hv)$  for Al doped ZnO thin films deposited with different Al content

**Table 2** The band gap energy values, NBE and DL emission in PL spectra

| Al content (%) | Eg (eV) | NBE emission (eV) | DL emission (eV) |
|----------------|---------|-------------------|------------------|
| 0              | 3.14    | 3.14              | 2.83             |
| 1              | 3.15    | 3.15              | 2.83             |
| 2              | 3.16    | 3.16              | 2.83             |
| 3              | 3.18    | 3.17              | 2.84             |
| 4              | 3.19    | 3.19              | 2.84             |
| 5              | 3.20    | 3.19              | 2.84             |

absorption edge exhibits a blue shift with doping of Al. The blue shift in the absorption edge can be related to the filling of the small density of states and the enhancement of carrier concentration in the AZO thin films. This phenomenon is known as the Burstein–Moss (BM) effect [38]. In fact, with doping of Al in ZnO, the carrier concentration increases, Fermi level shifts to conduction band and then the band gap value increases [41, 42]. More explanations about the increasing of carrier concentration due to Al doping into ZnO will be discussed in Sect. 3.4.

On the other hand, the displacement of the absorption edge of the ZnO with Al doping can be observed significantly at wavelength smaller than 400 nm. These results indicate that the produced AZO thin films can be used in photovoltaic applications due to the sharp enhancement of absorbance in the strong absorption region.

### 3.3 Photoluminescence

Figure 6a shows the photoluminescence (PL) spectra of AZO thin films deposited by different Al doping values which are measured in room temperature. The PL spectra

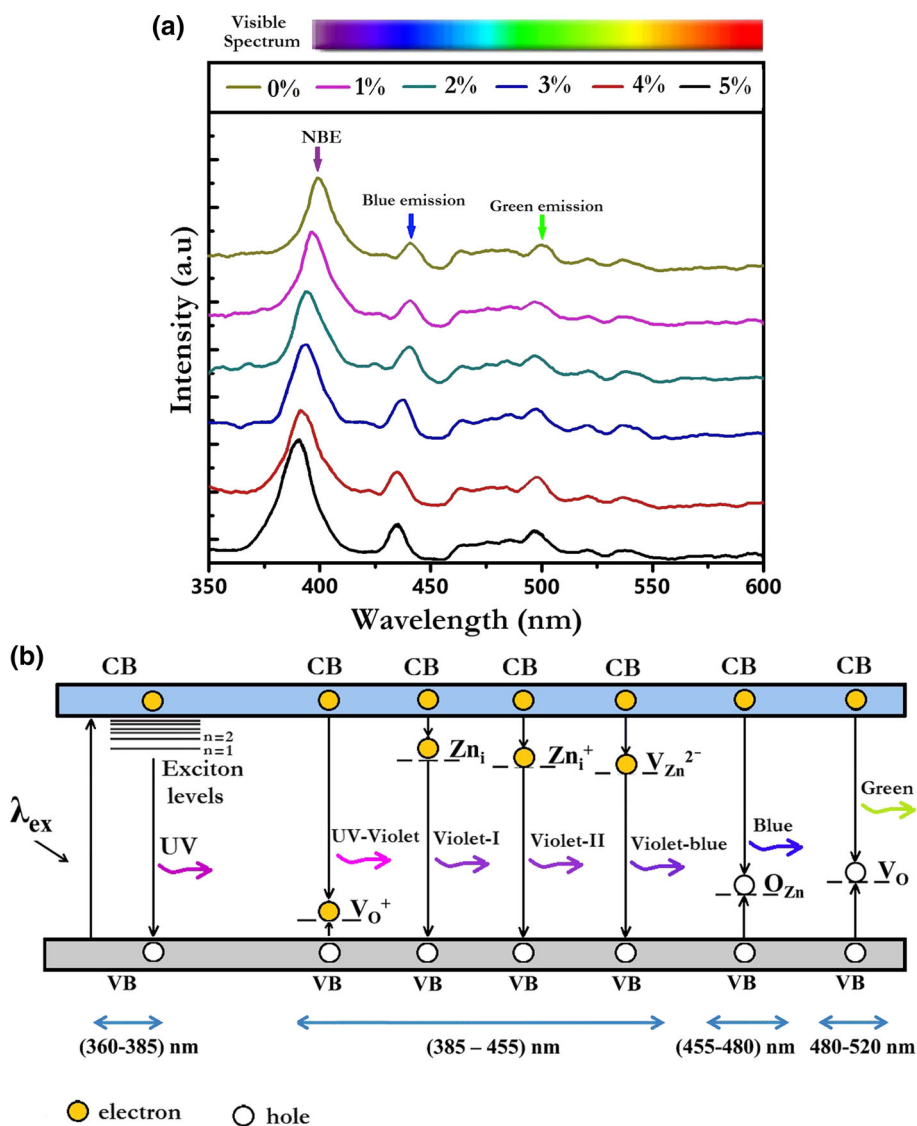
of AZO thin films are featured by a near band edge (NBE) emission in the ultraviolet region, and two peaks in blue and green region due to deep-level emission (DLE). Figure 6b presents a schematic of energy levels of the usual defects in ZnO thin films. As shown in Fig. 6b the NBE emission can be related to the free exciton recombination near to band gap while the DLE is attributed to the presence of defects in ZnO lattice, such as Zn vacancies, interstitials, and oxygen vacancies [19]. As it can be seen from Fig. 6a, the enhancement of Al doping concentration leads to the increasing of NBE and DLE intensities of peaks. The increasing of these intensities are mainly due to the enhancement of defects in ZnO lattice and the reduction of crystal quality [43, 44].

From the PL spectra, it can be seen that the NBE peak of the undoped ZnO thin film is centered at 3.14 eV (395 nm). Also the blue and green emissions are centered at 2.83 eV (438 nm) and 2.50 eV (496 nm) respectively. The site of NBE and DLE peaks for the ZnO and Al doped ZnO are given in Table 2. Presented results in Table 2 revealed that the NBE peak shifts to shorter wavelengths (blue shift) with the enhancement of Al doping, while the DLE peaks doesn't shift significantly as the increasing of Al doping level. A blue shifting of the NBE peak with the increasing of Al doping levels can be related to Moss-Burstein effect [33, 36]. It is known that the replacement of  $Zn^{2+}$  by  $Al^{3+}$  ions in AZO nanostructures leads to increase the Fermi level and then the broadening of optical band gap, which causes a blue shift in NBE peak. The calculated energy gap values from Tauc formula in pervious section confirm this blue shift. Similar results are reported by other researchers [45, 46].

### 3.4 Electrical properties

The electrical resistivity ( $\rho$ ), the mobility ( $\mu$ ), and the carrier concentration ( $n$ ) of the AZO thin films as a function of Al doping value are shown in Fig. 7. As it is shown in Fig. 7, the electrical resistivity decreases as Al content increases from 0 to 3 % while with further increasing of Al doping value from 3 to 5 % the electrical resistivity enhances. Also presented results in Fig. 7 reveals the enhancement of mobility and charge carrier concentration with increasing of Al content from 0 to 3 % and then reduction of these parameters with more Al doping value. The reduction of electrical resistivity and increasing of the charge carrier concentration at low Al doping value can be related to the free electrons generation due to the enhancement of  $Al^{3+}$  ions into ZnO lattice. However, at high Al doping values the excess Al ions occupy interstitial sites instead of substitution sites, result in more defects in ZnO lattice, and thus the reduction of mobility and charge carrier concentration [33, 47].

**Fig. 6 a** The room temperature PL spectra of samples deposited with different Al content, **b** energy levels of the defects in ZnO thin films



**3.5 FESEM results**

For all the samples deposited with different Al doping values, the top and cross sectional FESEM micrographs are shown in Fig. 8. It can be seen from FESEM images that the Al doping value plays an important role in the morphological properties of AZO thin films deposited on FTO substrate. Figure 8 shows a decrease in the size of the grains/clusters with increasing the Al doping value. The reduction of grain size with increasing the Al content is consistent with the results obtained from XRD patterns.

**3.6 AFM results**

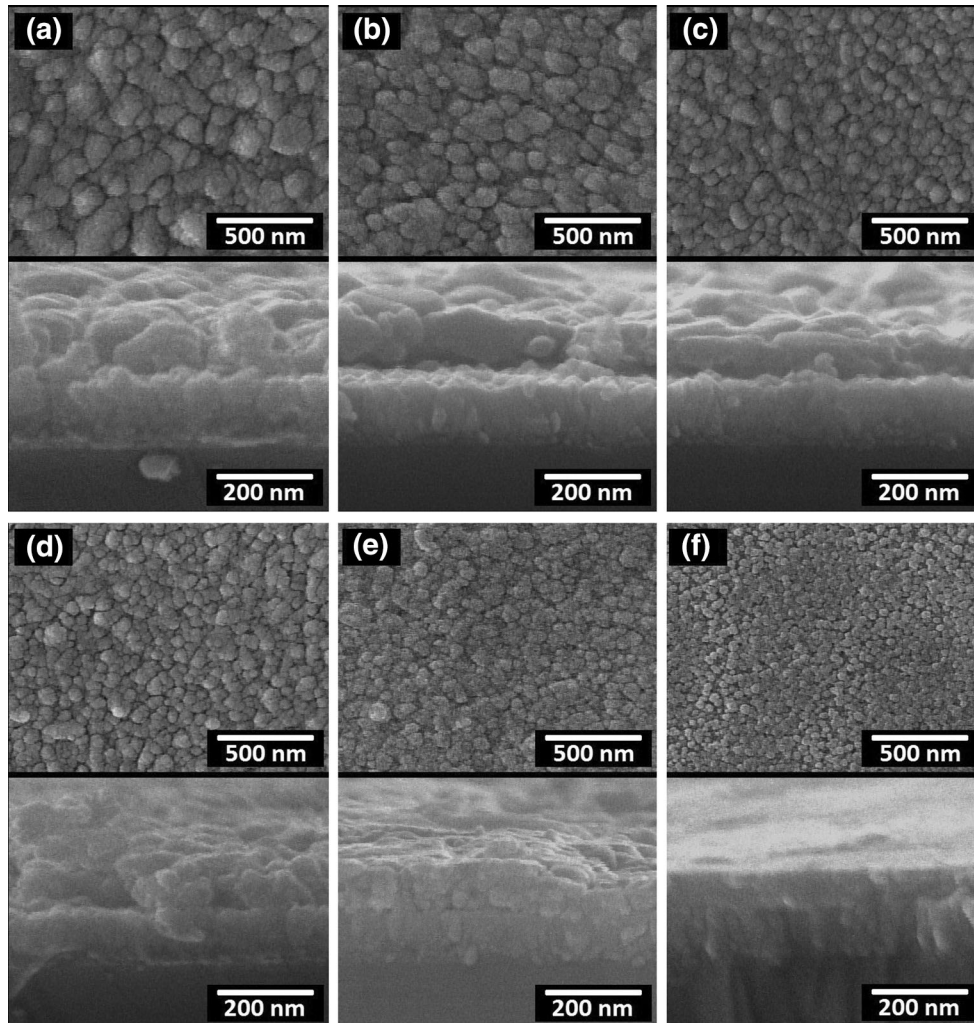
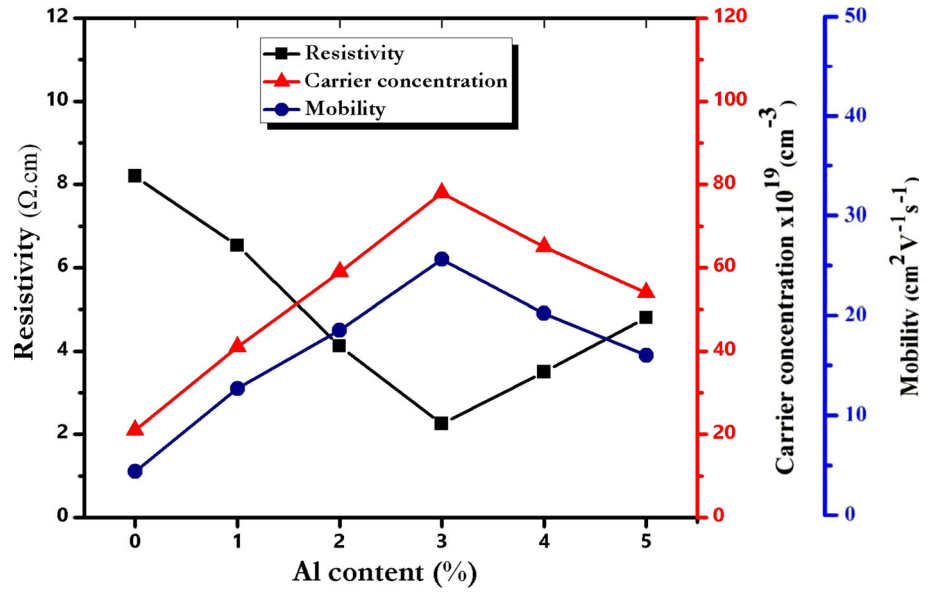
Figure 9 shows the AFM images (2D and 3D) of the AZO thin films deposited on FTO substrates with various Al doping levels. All AFM images are obtained in a scanning

area of  $3 \mu\text{m} \times 3 \mu\text{m}$ . Also the histograms of distribution of the grain sizes on the AZO surface deposited with different Al doping levels are presented in Fig. 9. As it can be seen from the grain size distribution histograms, when Al is doped in ZnO the histograms show a decrease in the size of the most of the grains. Indeed, the modes of the distributions (their peak points) vary from 64 to 61, 41, 37, 34 and then 21 nm for the thin films deposited with 0, 1, 2, 3, 5 and 5 % Al content, respectively.

As it was already mentioned, it can be due to the fact that ionic radius of the substitution element ( $\text{Al}^{3+}$  ions) is smaller than the host element ( $\text{Zn}^{2+}$ ), and therefore the size of the grains on the surface of the AZO thin films gets smaller as Al doping value increases.

To analyze and compare the surface roughness of the AZO deposited thin films, in each experiment, the roughness of three random areas over the surface of sample

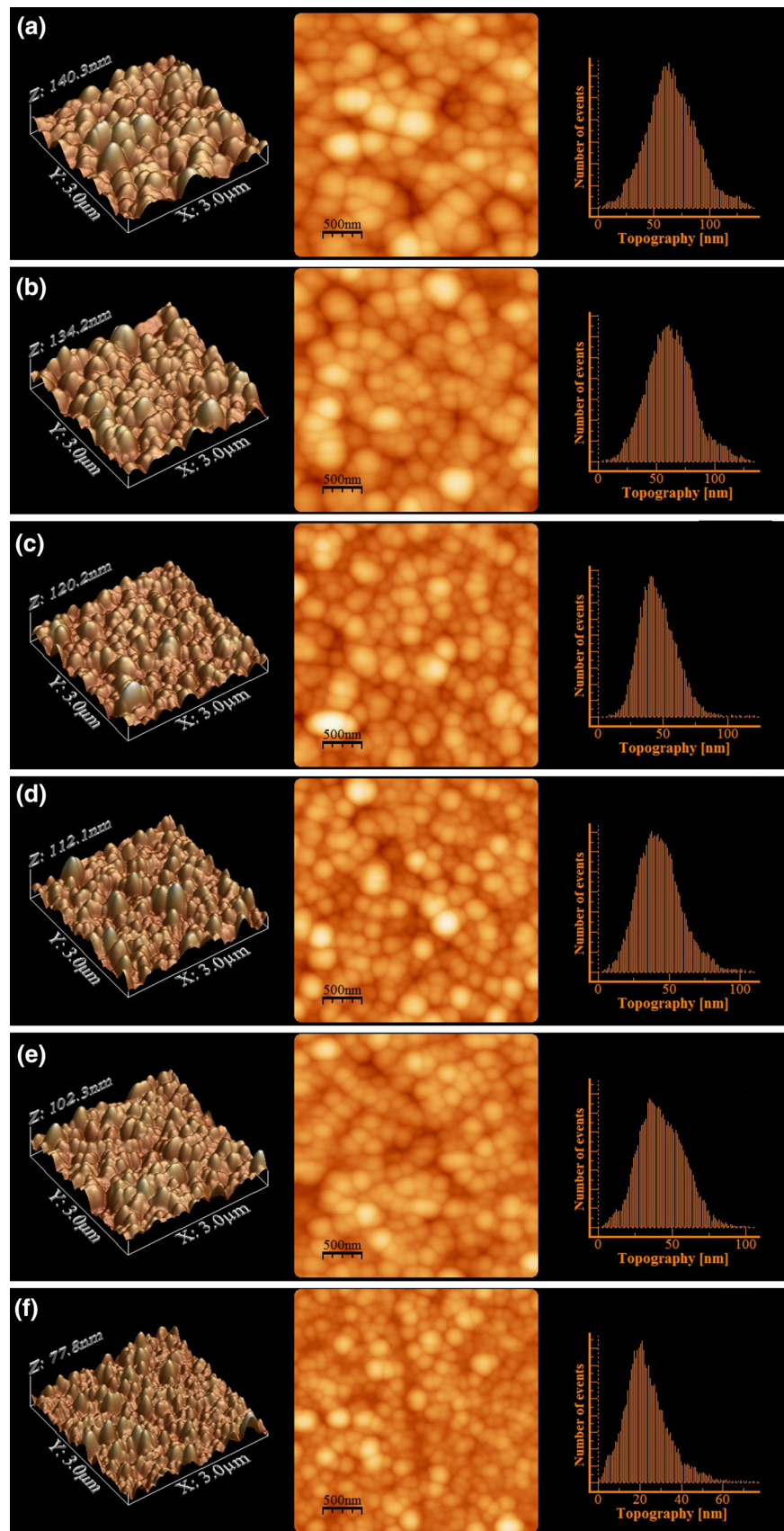
**Fig. 7** The electrical resistivity, mobility and carrier concentration of the Al doped ZnO thin films deposited with different Al content



**Fig. 8** The cross sectional and top view of the FESEM images of Al-doped ZnO films deposited with **a** 0 %, **b** 1 %, **c** 2 %, **d** 3 %, **e** 4 % and **f** 5 % Al content



**Fig. 9** 2D and 3D AFM micrographs and histograms of distribution of size of grains on the surface of the Al doped ZnO thin films deposited with **a** 0 %, **b** 1 %, **c** 2 %, **d** 3 %, **e** 4 % and **f** 5 % Al content



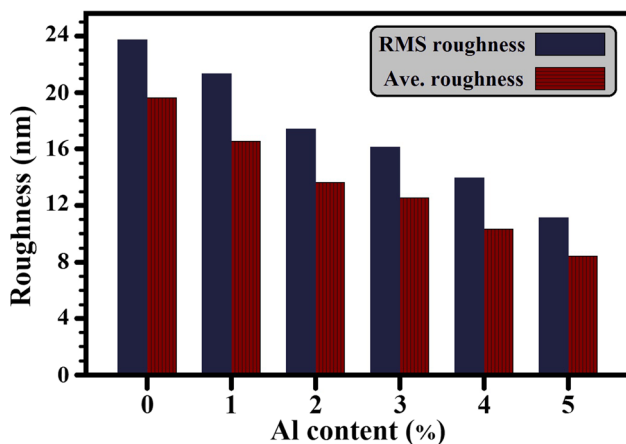


**Fig. 10** Average and RMS surface roughness of the Al doped ZnO thin films deposited with different Al content

measured, and the average and root means square (rms) roughness values of the measurements recorded. The recorded average and rms values of the roughness measurements are plotted versus the Al content and shown in Fig. 10. As it can be seen from Fig. 10, the average and rms roughness reduce with increasing the Al doping value. This is consistent with our previously mentioned general explanation: the enhancement of Al doping value leads to decrease the size of the grains on the surface and then the surface roughness reduces. The FESEM results clearly confirm the presence of smaller grains/clusters on the surface of deposited samples with increasing the Al content.

#### 4 Conclusions

Al doped ZnO nanostructures were deposited on the FTO glass substrate by spray pyrolysis method. The structural, morphological, optical and electrical properties of the thin films deposited with various Al doping values were investigated. From XRD patterns it was found that Al doping level had a key role on crystal quality and preferred crystal orientation of AZO thin films. The AZO films deposited with lower Al doping values showed a preferred crystal orientation along the (002) plane, However the preferred crystal orientation changed from (002) to (101) with the enhancement of Al doping level from 3 to 5 wt%. AFM results indicated that surface roughness and the size of the grains on the surface of the AZO films decrease as Al doping value increases. Also FESEM images confirmed that size of the grains/clusters decrease with increasing of Al doping level. The lowest resistivity and highest optical transmittance in the visible range were obtained for the sample deposited with 3 wt% Al doping value. Moreover,

the results of the optical transmittance and PL spectra revealed that the optical band gap and the defects in the AZO nanostructures can be control by varying the Al doping values. Also the displacement of the absorption edge of the ZnO with Al doping due to Moss-Burstein effect observed significantly at wavelength smaller than 400 nm. These results indicated that the produced AZO thin films can be used in photovoltaic applications due to the sharp enhancement of absorbance in the strong absorption region.

#### References

1. K. Mahmood, D. Song, S.B. Park, *Surf. Coat. Technol.* **206**, 4730 (2012)
2. K. Ravichandran, R. Mohan, N.J. Begum, K. Swaminathan, C. Ravidhas, *J. Phys. Chem. Solids* **74**, 1794 (2013)
3. M. Shirazi, M.T. Hosseini, A. Zandehnam, M. Ghoranneviss, G.R. Etaati, *J. Alloys Compd.* **602**, 108 (2014)
4. F. Zahedi, R.S. Dariani, S.M. Rozati, *Sens. Actuators A Phys.* **199**, 123 (2013)
5. X. Yu, X. Yu, J. Zhang, Z. Hu, G. Zhao, Y. Zhao, *Sol. Energy Mater. Sol. Cells* **121**, 28 (2014)
6. S. Yun, J. Lee, J. Chung, S. Lim, *J. Phys. Chem. Solids* **71**, 1724 (2010)
7. Y. Houand, A.H. Jayatissa, *Thin Solid Films* **562**, 585 (2014)
8. X.Y. Du, Y.Q. Fu, S.C. Tan, J.K. Luo, A.J. Flewitt, S. Maeng, S.H. Kim, Y.J. Choi, D.S. Lee, N.M. Park, J. Park, W.I. Milne, *J. Phys. Conf. Ser.* **76**, 012035 (2007)
9. F. Fleisshaker, V. Wloka, I. Hennig, *J. Mater. Chem.* **20**, 6622 (2010)
10. H. Gullapalli, V.S.M. Vemuru, A. Kumar, A. Botello-Mendez, R. Vajtai, M. Terrones, S. Nagarajiah, P.M. Ajayan, *Small* **16**, 1641 (2010)
11. S. Kim, G. Nam, H. Park, H. Yoon, S. Lee, J.S. Kim, J.S. Kim, D.Y. Kim, S.O. Kim, J.Y. Leem, *Bull. Korean Chem. Soc.* **34**, 1205 (2013)
12. C. Feng, W. Yi-Ding, Y. Jing-Zhi, C. Meng-Long, H. Liang-Yu, *Chin. Phys. Lett.* **26**, 114203 (2009)
13. A. Bouaoud, A. Rmili, F. Ouachtari, A. Louardi, T. Chtouki, B. Elidrissi, H. Erguig, *Mater. Chem. Phys.* **137**, 843 (2013)
14. N.H. Hashim, S. Subramani, M. Devarajan, *J. Mater. Sci. Mater. Electron.* **27**, 3520 (2016)
15. O. Gurbuz, S. Guner, *Ceram. Int.* **41**, 3968 (2015)
16. J. Perrenoud, L. Kranz, S. Buecheler, F. Pianezzi, A.N. Tiwari, *Thin Solid Films* **519**, 7444 (2011)
17. S. Zhao, Y. Zhou, K. Zhao, Z. Liu, P. Han, S. Wang, W. Xiang, Z. Chen, H. Lu, B. Cheng, G. Yang, *Phys. B* **373**, 154 (2006)
18. J. Chen, J. Chen, D. Chen, Y. Zhou, W. Li, Y. Ren, L. Hu, *Mater. Lett.* **117**, 162 (2014)
19. L. Dejam, S.M. Elahi, H.H. Nazari, H. Elahi, S. Soleymani, A. Ghaderi, *J. Mater. Sci. Mater. Electron.* (2015). doi:10.1007/s10854-015-3804-7
20. C.M. Muiva, T.S. Sathiaraj, K. Maabong, *Ceram. Int.* **37**, 555 (2011)
21. J. Xu, H. Wang, L. Yang, M. Jiang, S. Wei, T. Zhang, *Mater. Sci. Eng. B* **167**, 182 (2010)
22. B.J. Babu, A. Maldonado, S. Velumani, R. Asomoza, *Mater. Sci. Eng. B* **174**, 31 (2010)

23. Y.S. Jung, H.W. Choi, K.H. Kim, J. Korean Phys. Soc. **55**, 1945 (2009)
24. O. Gurbuz, I. Kurt, S. Caliskan, S. Guner, Appl. Surf. Sci. **349**, 549 (2015)
25. H.W. Park, K.B. Chung, J.S. Park, S. Ji, K. Song, H. Lim, M.H. Jang, Ceram. Int. **41**, 1641 (2015)
26. A.A. Al-Ghamdi, O.A. Al-Hartomy, M. El-Okr, A.M. Nawar, S. El-Gazzar, F. Yakuphanoglu, Spectrochim. Acta A **131**, 512 (2014)
27. A. Monemdjou, F.E. Ghodsi, J. Mazloom, Superlattices Microstruct. **74**, 19 (2014)
28. K.C. Park, D.Y. Ma, K.H. Kim, Thin Solid Films **305**, 201 (1997)
29. H. Benzarouk, A. Drici, M. Mekhnache, A. Amara, M. Guerioune, JCh. Bernede, Superlattices Microstruct. **52**, 594 (2012)
30. B.D. Cullity, S.R. Stock, *Elements of X-ray diffraction*, 3rd edn. (Prentice-Hall, New York, 2001)
31. L. Castañeda, R. Silva-González, J.M. Gracia-Jiménez, M.E. Hernández-Torres, M. Avendaño-Alejo, C. Márquez-Beltrán, M. de la L. Olvera, J. Vega-Pérez, A. Maldonado, Mater. Sci. Semicond. Process **13**, 80 (2010)
32. B. Joseph, P.K. Manoj, V.K. Vaidyan, Ceram. Int. **32**, 487 (2006)
33. M. de la L. Olvera, A. Maldonado, J. Vega-Pérez, O. Solorza-Feria, Mater. Sci. Eng. B **174**, 42 (2010)
34. T.V. Vimalkumar, N. Poornima, K.B. Jinesh, C.S. Kartha, K.P. Vijayakumar, Appl. Surf. Sci. **257**, 8334 (2011)
35. Z. Pan, X. Tian, S. Wu, X. Yu, Z. Li, J. Deng, C. Xiao, G. Hu, Z. Wei, Appl. Surf. Sci. **265**, 870 (2013)
36. M. Caglar, S. Ilican, Y. Caglar, F. Yakuphanoglu, J. Mater. Sci. Mater. Electron. **19**, 704 (2008)
37. M.C.E. Benouis, M.S. Aida, A.S. Juarez, F. Yakuphanoglu, A.T. Silver, J. Alloys Compd. **506**, 548 (2010)
38. C.S. Prajapati, A. Kushwaha, P.P. Sahay, Mater. Chem. Phys. **142**, 276 (2013)
39. L. Dghoughi, F. Ouachtari, M. Addou, B. Elidrissi, H. Erguig, A. Rmili, A. Bouaoud, Phys. B **405**, 2277 (2010)
40. Z.W. Li, W. Gao, R.J. Reeves, Surf. Coat. Technol. **198**, 319 (2005)
41. Q. You, H. Cai, Z. Hu, P. Liang, S. Prucnal, Sh Zhou, J. Sun, N. Xu, J. Wu, J. Alloys Compd. **644**, 528 (2015)
42. B.E. Sernelius, Phys. Rev. B **37**, 10244 (1988)
43. F. Ramos-Brito, C. Alejo-Armenta, M. Garcia-Hipolito, E. Camarillo, J. Hernandez, C. Falcony, H. Murrieta, J. Lumin. **131**, 874 (2011)
44. J. Sengupta, R.K. Sahoo, C.D. Mukherjee, Mater. Lett. **83**, 84 (2012)
45. C.W. Chen, K.H. Chen, C.H. Shen, A. Ganguly, L.C. Chen, J.J. Wu, H.I. Wen, W.F. Pong, Appl. Phys. Lett. **88**, 241905 (2006)
46. S. Yun, J. Lee, S. Lim, Phys. B **405**, 413 (2010)
47. R. Pandey, S. Yuldashev, H.D. Nguyen, H.C. Jeon, T.W. Kang, Curr. Appl. Phys. **12**, S56 (2012)